Springer

Journal of Mechanical Science and Technology 22 (2008) 1870~1875

Journal of Mechanical Science and Technology

www.springerlink.com/content/1738-494x
DOI 10.1007/s12206-008-0725-x

Numerical analysis for prediction of flow rate of the motor cooling fan †

Tae In Kang, Cheol O Ahn, In Soo Seo and Sang Hwan Lee*

Department of Mechanical Engineering, Hanyang University, 17 Haengdang-dong, Seoul 133-791, Korea

(Manuscript Received April 16, 2008; Revised June 20, 2008; Accepted July 23, 2008)

Abstract

In this study, we analyzed the three dimensional unsteady flow around a motor cooling fan using the vortex panel method. For a popular type of motor cooling fan that has thin blades, we predicted the flow rate through numerical analysis without experimental data, such as the free stream velocity, which is a boundary condition of the flow field. We also calculated the flow rate for various cooling fan geometries and rotating speeds. For these fans, the numerical results showed flow rates within 3% of the experimental results.

Keywords: Motor cooling fan; Unsteady lifting surface theory; Time stepping method; Free stream velocity

1. Introduction

Recently, the electric motor has demonstrated the problem of increased caloric usage due to its massive volume and high speed. The development of an efficient cooling system for fan motors has a direct influence on enhancing motor reliability and lifetime. For the radiation system of a general motor, the cooling fan plays a very important role.

Because the motor must have identical cooling performance for forward or reverse rotations, the motor cooling fan typically is of the radial type. Because radial fans, unlike axial fans, have a very complex flow field, a three-dimensional analysis is essential. However, it is not easy to analyze the three-dimensional flow of radial fans using general computational techniques. If we analyze the flow with commercial CFD software, boundary conditions such as velocity and pressure at the inlet and outlet must be defined. If no information about the boundary conditions is available, it is very difficult to predict the flow rate at an operation point.

In this study, we attempted to design a program to predict the flow rate without specific inlet and outlet boundary conditions.

Specifically, we only used the fan geometries and rotating speed to predict the flow rate.

In this study, we composed a flow field using the unsteady lifting surface theory [1-8] and analyzed the flow field using the vortex panel method [8]. In order to verify the results of the numerical analysis, we compared the numerical analysis results with the flow rate data gathered by experiment. Fig. 1 denotes an

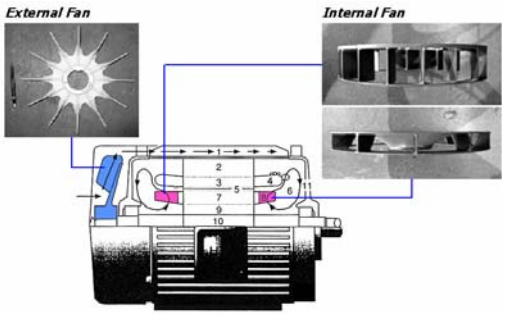

Fig. 1. The motor and cooling fan (external fan and internal fan).

† This paper was presented at the 9th Asian International Conference on Fluid Machinery (AICFM9), Jeju, Korea, October 16-19, 2007.

*Corresponding author. Tel.: +82 2 2220 0445, Fax.: +82 2 2220 0445
E-mail address: shlee@hanyang.ac.kr

external fan inside a generic motor.

2. Numerical method

2.1 Vortex panel method

Because the flow field around motor cooling fans has a very high Reynolds number at the operation point, the flow field around the fans has a very thin boundary layer. Moreover, the viscous effect is restricted in this thin boundary layer and the separating wake. Therefore we assumed that the flow field could be represented by potential flows which are incompressible and irrotational. Lastly, the flow must be satisfied following Laplace's equation.

$$\nabla^2\phi = 0 \tag{1}$$

In order to solve the above Eq. (1), we need to apply the following four boundary conditions. [8]

(a) The Flow tangency condition:

$(\nabla\phi + \vec{V}_\infty)\cdot\vec{n} = 0 \quad \Rightarrow \quad \nabla\phi\cdot\vec{n} = -(\vec{V}_\infty\cdot\vec{n})$

(b) The Kutta-condition: $\gamma_{T.E.} = 0$

(c) $\nabla\phi = 0$, as $\mathrm{r}\to\infty$

(d) The Force-free condition: $\Delta\vec{F} = \rho\vec{V}_\infty \times \vec{\gamma}_W = 0$

In boundary conditions, $\vec{V}_\infty$ is the free stream velocity, $\vec{n}$ is unit normal vector at the lifting surface, and γ is the vortex strength. When a body is located at an arbitrary point, $P(x,y,z)$, in the flow field, the potential velocity is reflected by Eqs. (2)-(4).

$$\begin{aligned}\phi(p) = &-\frac{1}{4\pi}\int_{Body}\left[\sigma\left(\frac{1}{r}\right) - \mu\vec{n}\cdot\nabla\left(\frac{1}{r}\right)\right]ds \\ &+\frac{1}{4\pi}\int_{Wake}\left[\mu\vec{n}\cdot\nabla\left(\frac{1}{r}\right)\right]ds + \phi_\infty(p)\end{aligned} \tag{2}$$

$$r = \sqrt{(x-x_0)^2 + (y-y_0)^2 + (z-z_0)^2} \tag{3}$$

$$\phi_\infty(p) = U_\infty + V_\infty + W_\infty \tag{4}$$

In the above Eq. (2), σ is the source strength and μ is the doublet strength. r is the distance between specified points and an arbitrary point (p) in the flow field, ds is the lifting surface area, ϕ_∞ is the potential velocity of a free stream, and $(U_\infty + V_\infty + W_\infty)$ is the velocity component of the free stream velocity. [8]

2.2 Distribution of lifting surface

The unsteady lifting surface theory is useful to analyze the three dimensional flow field around the thin fan wings. Therefore, in order to solve the flow field governing equation, the specifiable elements of the lifting surface are distributed in the flow field following the shape of a body using this theory.

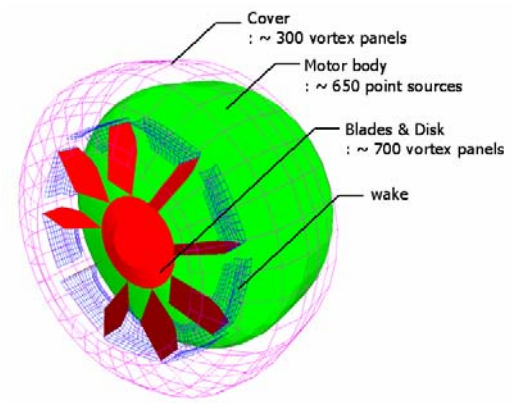

Fig. 2. Geometry of a motor cooling fan expressed as panels (modeling of an external fan, cover, and motor body).

The lifting surface is composed of many panels. Each panel is composed of four straight vortex segments. Hence, a panel forms a quadrilateral. The collocation points, which must be satisfied by the boundary conditions, are located at the center of each panel. The panel strength is determined by application of the flow-tangency condition, and it is proportional to the difference in normal velocity. Fig. 2 describes a motor expressed as panels.

2.3 Aerodynamic influence coefficient

The Aerodynamic Influence Coefficient (AIC) is specified by the body geometry. AIC is defined by the normal velocity components induced by unit vortex strength of panels distributed on the surface of a body [8].

Specifically, AIC is the normal velocity component induced by j panels, which have unit-strength at the collocation point of the i th panel. Therefore,

$$a_{ij} \quad = \quad (u,\ v,\ w)_{ij}\cdot\mathbf{n}_i \tag{5}$$

where, a_{ij} is the AIC, $\mathbf{n}_i$ is the unit normal velocity at the i th panel, and $(u,\ v,\ w)_{ij}$ is the velocity induced by j th panels at the specified collocation points.

In the flow field, the velocity at an arbitrary point is determined by the velocity induced by the vortex segment of a panel. The velocity is calculated by the

Biot-Savart law [8], which is

$$\Delta\vec{q} = \frac{\Gamma}{4\pi}\frac{d\vec{l}\times\vec{r}}{\vec{r}^{3}}. \tag{6}$$

The above Eq. (6) becomes

$$\vec{q}_{1,2} = \frac{\Gamma}{4\pi}\frac{\vec{r}_1\times\vec{r}_2}{\left|\vec{r}_1\times\vec{r}_2\right|^2}\left(\vec{r}_1-\vec{r}_2\right)\cdot\left(\frac{\vec{r}_1}{r_1}-\frac{\vec{r}_2}{r_2}\right) \tag{7}$$

$$r_1 = \sqrt{\left(x_p-x_1\right)^2+\left(y_p-y_1\right)^2+\left(z_p-z_1\right)^2}$$

$$r_2 = \sqrt{\left(x_p-x_2\right)^2+\left(y_p-y_2\right)^2+\left(z_p-z_2\right)^2},$$

while the velocity induced by a point source is

$$\vec{q} = \frac{\sigma}{4\pi}\frac{\vec{r}\times\vec{r}_0}{\left|r-r_0\right|^3}. \tag{8}$$

2.4 Application of boundary condition

The strength of each panel is determined by the application of a flow-tangency condition. The velocity at an arbitrary point is composed of the velocities induced by the body panels, wake panels, motion of the body, and free stream velocity. The sum of the velocities from multiple points must be zero to satisfy the flow tangency condition, which is

$$\begin{aligned}&\mathrm{a}_{i1}\Gamma_1+\mathrm{a}_{i2}\Gamma_2+\cdots\cdots+\mathrm{a}_{ii}\Gamma_i\\&+\left[U(t)+u_w,\ \ V(t)+v_w,\ \ W(t)+w_w\right]_i\cdot\mathrm{n}_i=0\end{aligned} \tag{9}$$

The above Eq. (9) results in a set of algebraic equations with the unknown Γ_i;

$$\begin{bmatrix} a_{11} & a_{12} & a_{13} & a_{14} & \cdots & a_{1j}\\ a_{21} & a_{22} & a_{23} & a_{24} & \cdots & a_{2j}\\ \vdots & \vdots & \vdots & \vdots & & \vdots\\ a_{i1} & a_{i2} & a_{i3} & a_{i4} & \cdots & a_{ij}\end{bmatrix}\begin{bmatrix}\Gamma_1\\ \Gamma_2\\ \vdots\\ \Gamma_i\end{bmatrix} = -\begin{bmatrix} RHS_1\\ RHS_2\\ \vdots\\ RHS_i\end{bmatrix} \tag{10}$$

The above matrix has a well-defined diagonal and can be solved using linear algebra.

In Eq. (10), a_{ij} describes the AIC, while RHS_i is determined by the induced velocity caused by the wake, motion of the body, and free stream. The RHS_i of i th specification element is

$$RHS_i = \left[U(t)+u_w, V(t)\_v_w, W(t)+w_w\right]\cdot\mathbf{n}_i \tag{11}$$

In above Eq. (11), $\left[U(t),\ V(t),\ W(t)\right]$ is the velocity induced by motion of the body and free stream, while $\left[u_w,\ v_w,\ w_w\right]_i$ is the velocity induced by the wake.

The above matrix must be solved for every time step because the RHS continues to change.

3. Results and considerations

3.1 Experiment

In order to verify the numerical results, for five fans (A0, A1, A2, A3, A4) we measured the flow rate with a chamber type fan tester, the specifications of which are shown in Table 1.

To verify the numerical results, flow rate measurements for various fan blade shapes and speeds were conducted. Namely, the flow rate was measured by a test chamber with a multiple nozzle type fan tester built ANSI/AMCA Standard 210-85 and ASHRAE Standard 51-85.

In order to improve the flow rates for the considered fans we redesigned the shape of each blade (Fig. 3). A0 is a commercial motor cooling fan that has a diameter of 222 mm. The other fans were made to compare directly with A0, and their diameters were specified to be 222 mm. The fan disk and blades were manufactured individually so that easy assembly would be possible. Fig. 4 denotes an assembled external fan.

Table 1. Specification of fan tester.

Chamber type fan tester	
Differential pressure transmitter	DRUCK LPX5480 (0~+100mmAq)
	DRUCK LPX5480 (-50~+50mmAq)
Torque converter	Ono Sokki TS-2600
Torque detector	Ono Sokki SS-501
Data acquisition system	National Instrument PCI-6024E / SCB-68
Driving unit	Inverter Controlled 3.0HP

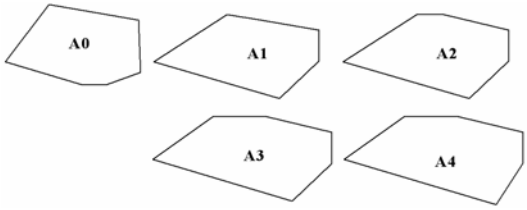

Fig. 3. The plans of each external fan blade (blade shapes for A0, A1, A2, A3, and A4).

Fig. 4. Development of the wake.

3.2 Execution of numerical analysis

3.2.1 Modeling of wake

In this study, in order to determine the wake motion, we applied a Time Stepping Method that can be used to analyze three-dimensional unsteady flow and does not need initial data to form the wake.

This is a method that determines positions by calculating the local velocity and wake development at every time step. The wake is expressed by panels that have a given strength, and it is separated from the trailing edge of the blade. The strength of each wake panel is defined by the Kutta-condition.

$$\Gamma_{w_i} = -\Gamma_{T.E_{t-\Delta t}} \tag{12}$$

where, $\Gamma_{T.E}$ is the strength at the trailing edge of the blade and Γ_w is the strength of the wake separated from the trailing edge of the blade. Fig. 5 shows a developing wake as time passes.

The strength of the wake panels does not change according to Helmholtz's law. Hence the wake is moved downstream by local velocity. The local velocity is expressed by

$$(u,v,w)_i = (u,v,w)_{Body} + (u,v,w)_{Wake} + (u,v,w)_{\infty}, \tag{13}$$

while the movement distance is noted as

$$(\Delta x, \Delta y, \Delta z) = (u,v,w)\cdot \Delta t\,. \tag{14}$$

$$\Delta t = \frac{\Delta \phi}{\omega} \tag{15}$$

where, $\Delta\phi$ is rotation range (rad) and ω is angular velocity (rad/s).

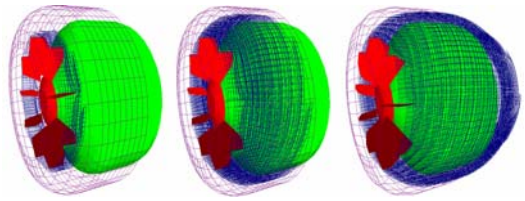

Fig. 5. Motor with the A0 fan blade design.

3.2.2 Determination of free stream velocity

The RHS is updated at every time step. Since the RHS includes the free stream velocity, it results in a change of flow field strength. The strength of the wake panels that separate at the trailing edge of blade is determined by the Kutta-condition. In this study, the calculated initial free stream velocity was applied to the flow field.

During the velocity field is convergence the induced velocity at inlet was calculated by the strength of wake panels. The induced velocity was applied to the calculation at every time step. The free stream velocity is calculated by

$$U_{\infty}^{new} = \sum_i u_{wake}(\Delta A_i)/A \tag{16}$$

where, U_{∞}^{new} is the free stream velocity updated at every time step, ΔA_i is the area per a grid at inlet, and A is the total inlet area. Lastly, the free stream velocity and strength of wake panels affect each other in the numerical system at every time step.

3.2.3 Calculation of flow rate

The flow rate is defined by the inlet area and inlet axial velocity component. This inlet velocity induced by all elements in the flow field is

$$u_i = u_{blade} + u_{cover} + u_{motor\,body} + u_{wake}\,, \tag{17}$$

while the flow rate is

$$Q = \sum_i u_i(\Delta A_i) \tag{18}$$

where, Q is flow rate, ΔA_i is the area per grid at the inlet, and u_i is the inlet velocity induced in the axial direction. During invariable iteration, if the maximum change of free stream velocity converges within 0.01 we assumed that the flow rate converged as shown in (19).

$$\frac{\left|\max\left(U_{\infty}^{i}\right)-\min\left(U_{\infty}^{j}\right)\right|_{past\ N}}{\overline{U_{\infty}}}<0.01 \quad (19)$$

3.3 Result and consideration of numerical analysis

Fig. 2 is a fan model in which the cover diameter is 310 mm and the fan diameter is 222 mm. Fig. 3 shows the blade shapes considered for A0, A1, A2, A3, and A4. Numerical analysis was performed for the geometry of each blade and rotating speed.

Fig. 6 is the flow rate convergence history at 1800 rpm for A0. Fig. 7 is the free stream velocity convergence history for A0 at 1800 rpm. In Fig. 6 and Fig. 7, when the initial free stream velocity is zero and 3 m/s, the flow rate converged to almost the identical value. The above results show that the predicted flow rate does not relate to the initial free stream velocity. Though the flow rate may be predicted without specific initial free stream velocity information, for velocity field stability, the initial free stream velocity was set to 3 m/s rather than zero. In other words, when the initial free stream velocity is 3 m/s, the velocity field is stabilized faster.

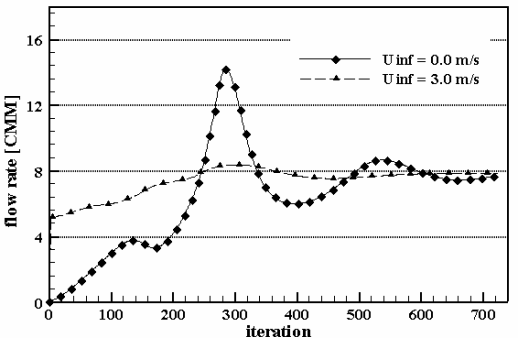

Fig. 6. Flow rate convergence history at 1800 rpm for A0.

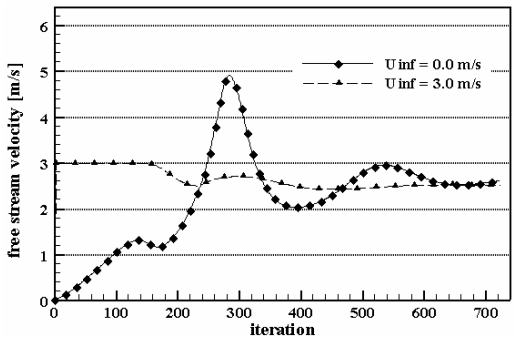

Fig. 7. Free stream convergences history at 1800 rpm for A0.

In light of these results, when the flow rate was predicted for all blade shapes and rotating speeds, the initial free stream velocity was set to 3 m/s.

Table 2 shows the predicted flow rate results for A1, A3, and A4 at 1500 rpm. A4 had the maximum flow rate among the considered fans. Table 3 contains the results of the predicted flow rates for A0, A1, and A2 at 1800 rpm. Figs. 8-11 show the convergence histories for each blade and rotating speed.

Table 2. Test results and CFD at 1500 rpm.

	Experiment [CMM]	Numerical [CMM]	Rel. Error [%]
A1	7.03	7.06	0.41
A3	7.12	7.25	1.70
A4	7.18	7.37	2.60

Table 3. Test results and CFD at 1800 rpm.

	Experiment [CMM]	Numerical [CMM]	Rel. Error [%]
A0	7.73	7.87	1.83
A1	8.46	8.50	0.47
A2	8.46	8.51	0.59

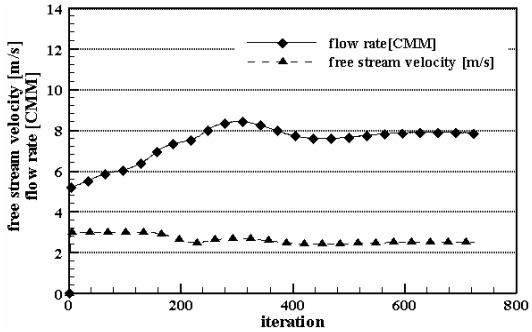

Fig. 8. Convergence history at 1800 rpm for A0.

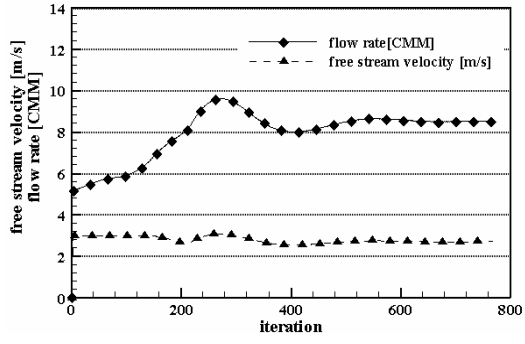

Fig. 9. Convergence history at 1800 rpm for A1.

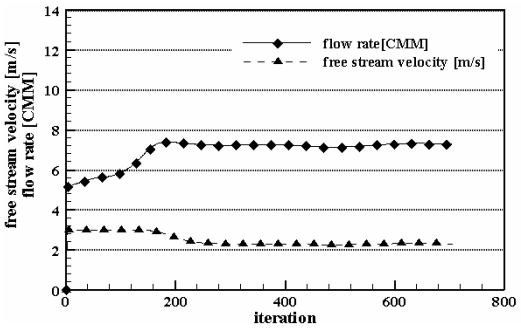

Fig. 10. Convergence history at 1500 rpm for A3.

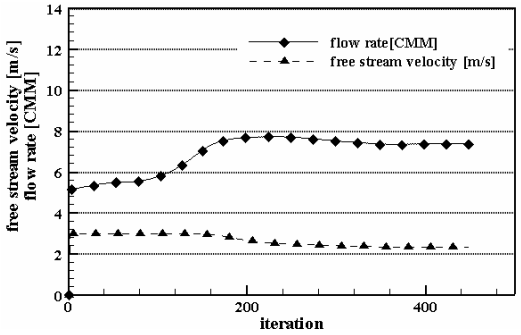

Fig. 11. Convergence history at 1500 rpm for A4.

From these results, we concluded that the velocity field is stable and that the flow rate converges with the free stream velocity.

4. Conclusion

From the results of this study, we developed the following conclusions.

(1) Our computational flow field includes the cover, body, and fan of the motor to predict the flow rate.

(2) We predicted the flow rate without the inlet and outlet boundary conditions by modeling.

(3) We successfully compared the flow rates for each blade and rotating speed.

(4) We can suggest improved shapes of motor cooling fans which have the maximum flow rate for a 222-mm diameter fan.

References

[1] Kussner, General Airfoil Theory, NACA TM-979 (1941).

[2] V. M. Falkner, The Calculation of Aerodynamic Load on Surface of Any Shape, Aeronautical Research Council R. & M. (1943) 1910.

[3] H. Multhopp, Methods for Calculating the Lift Distribution of Wings (Subsonic Lifting-Surface Theory), Aeronautical Research Council R. & M. (1950) 2884.

[4] M. T. Landahl, Kernel function for nonplanar oscillating surfaces in a subsonic flow, *AIAA Journal*, 5 (1967) 1045-1046.

[5] E. Albano and W. P. Rodden, A Doublet-Lattice method for calculating lift distribution on oscillating surfaces in subsonic flows, *AIAA Journal*, 7 **(**1969) 279-285.

[6] T. Ueda and E. H. Dowell, A new solution method for lifting surface in subsonic flow, *AIAA Journal*, 20 (1982) 348-355.

[7] T. Ueda and E. H. Dowell, Doublet-point method for supersonic unsteady lifting surfaces, *AIAA Journal*, 22 (1984) 179-186.

[8] J. Katz and A. Plotkin, Low Speed Aerodynamics-From Wing Theory to Panel Method, McGraw-Hill (1991).